Received: 19 January 2023 | Revised: 14 April 2023 | Accepted: 20 April 2023

DOI: 10.1111/cge.14352

ORIGINAL ARTICLE

CLINICAL GENETICS WILEY

Functional characterization of novel or yet uncharacterized *ATP7B* missense variants detected in patients with clinical Wilson's disease

Amelie Stalke[1,2] | Annika Behrendt[3] | Finja Hennig[1] | Holger Gohlke[3,4] | Nicole Buhl[1,2] | Thea Reinkens[1] | Ulrich Baumann[2] | Brigitte Schlegelberger[1] | Thomas Illig[5] | Eva-Doreen Pfister[2] | Britta Skawran[1]

[1]Department of Human Genetics, Hannover Medical School, Hannover, Germany

[2]Department of Pediatric Gastroenterology and Hepatology, Division of Kidney, Liver, and Metabolic Diseases, Hannover Medical School, Hannover, Germany

[3]Institute for Pharmaceutical and Medicinal Chemistry, Heinrich Heine University Düsseldorf, Düsseldorf, Germany

[4]Institute of Bio- and Geosciences (IBG-4: Bioinformatics), Forschungszentrum Jülich GmbH, Jülich, Germany

[5]Hannover Unified Bank, Hannover Medical School, Hannover, Germany

Correspondence
Amelie Stalke, Department of Human Genetics, Hannover Medical School, Carl-Neuberg-Str. 1, Hannover 30625, Germany.
Email: stalke.amelie@mh-hannover.de

Funding information
German Research Foundation (DFG), Grant/Award Number: #433387263; German Federal Ministry for Education and Research (BMBF) through HiChol, Grant/Award Number: 01GM1904A

Abstract

Wilson's disease (WD, MIM#277900) is an autosomal recessive disorder resulting in copper excess caused by biallelic variants in the *ATP7B* gene (MIM#606882) encoding a copper transporting P-type ATPase. *ATP7B* variants of unknown significance (VUS) are detected frequently, sometimes impeding a clear diagnosis. Functional analyses can help to classify these variants as benign or pathogenic. Additionally, variants already classified as (likely) pathogenic benefit from functional analyses to understand their pathomechanism, thus contribute to the development of personalized treatment approaches in the future. We described clinical features of six WD patients and functionally characterized five *ATP7B* missense variants (two VUS, three yet uncharacterized likely pathogenic variants), detected in these patients. We determined the protein level, copper export capacity, and cellular localization in an in vitro model and potential structural consequences using an ATP7B protein model based on AlphaFold. Our analyses give insight into the pathomechanism and allowed reclassification for the two VUS to *likely pathogenic* and for two of the three *likely pathogenic* variants to *pathogenic*.

KEYWORDS
ACMG classification, *ATP7B*, cellular localization, copper export, functional characterization, VUS, Wilson's disease

1 | INTRODUCTION

The autosomal recessive disorder Wilson's disease (WD) is caused by biallelic pathogenic variants in the *ATP7B* gene. The Cu(I)-transporting P-type ATPase ATP7B undergoes a catalytic copper transport cycle,[1] involving various protein domains and motifs. ATP7B has six highly conserved metal-binding domains (MBDs) at the N-terminus. Binding

Abbreviations: ACMG, American College of Medical Genetics and Genomics; ER, endoplasmic reticulum; ERAD, ER-associated degradation; MBD, metal-binding domain; TGN, trans-Golgi network; TMH, transmembrane helix; CNV, copy number variation; VUS, variant of unknown significance; WD, Wilson's disease.

of copper causes a conformational change that results in ATP binding to the nucleotide binding domain (N-domain).[2,3] The SEPHL motif within the N-domain is of particular importance for this. The N-terminally bound copper is brought into the vicinity of the ATPase's ion channel, which consists of eight transmembrane helices (TMH). The bound ATP then moves closer to the phosphorylation domain (P-domain).[4] Through the phosphorylation of a distinct catalytic aspartic acid residue (1027) in the P-domain's DKTG motif, the ion channel closes from the cytoplasmic side, facilitating the copper transport.[5] With the help of the actuator domain (A-domain), which has an intrinsic phosphatase activity in the TGE motif, the protein can be dephosphorylated so that the catalytic cycle can begin anew.[5]

Under physiological copper concentrations, ATP7B localizes in the trans-Golgi network (TGN) membrane, especially in the liver. There it transfers copper to ceruloplasmin to ensure that extrahepatic organs are supplied with the metal.[6] Under elevated copper concentrations, ATP7B is able to traffic to the apical hepatocyte membrane to remove copper excess into the bile.[7,8] Non-functional or absent ATP7B leads to copper accumulation, mainly in the liver and subsequently in the brain and other organs, thus WD primarily manifests with hepatic or neuropsychiatric abnormalities. However, the phenotype is highly variable in terms of disease onset, organ involvement, severity, and progression, and shows no correlation with the genotype.[9–11] The Leipzig Score can be used for clinical diagnosis, where WD is highly likely if the cumulative score is ≥4.[12] This scoring system also includes genetic analysis results. Genetic analyses occasionally detect variants with unknown impact, which have to be classified as variants of unknown significance (VUS) according to the criteria proposed by the American College of Medical Genetics and Genomics (ACMG).[13] Functional in vitro studies can help to reclassify such variants as benign or pathogenic and thus help to obtain a conclusive genetic diagnosis for patients with suspected WD.[14] They may also allow a better understanding of hypomorphic or incomplete penetrant variants, which have previously been attributed to *ATP7B*.[15,16] However, functional analyses are also useful for (likely) pathogenic variants, as they give deeper insights into their individual pathomechanism. This is often an important prerequisite for personalized therapies, which are desirable for WD. Current therapies such as D-penicillamine, zinc salts, trientine, or tetrathiomolybdate, can be very effective. However, they are often associated with side effects, poor compliance, high costs, and in some cases do not sufficiently address neurological symptoms and can even initially worsen them.[17,18] In this study, we functionally investigate five *ATP7B* variants of interest detected in six patients with clinically diagnosed WD and additionally describe their phenotypes.

2 | MATERIALS AND METHODS

2.1 | Subjects

At Hannover Medical School (MHH), six patients underwent diagnostic work-up for chronic liver disease and were identified by genetic analyses to have VUS or functionally uncharacterized likely pathogenic *ATP7B* variants. Clinical and laboratory investigations were highly suggestive of WD. All data for this manuscript was retrospectively collected from clinical case notes at MHH. The study protocol conforms to the ethical guidelines of the Declaration of Helsinki (1964) and has been approved by the MHH ethics committee (#7656-2018). Patients and/or parents gave written informed consent.

2.2 | Sequencing and copy number variation analysis

DNA was extracted from whole blood samples. DNA enrichment and library preparation were performed using the xGen® Exome Research Panel (IDT, Inc., Coralville, USA) or custom panel V04 (IDT) covering the *ATP7B* coding region with at least ±20 bases of exon/intron boundaries and the *ATP7B* 5'UTR. Sequencing was performed on a NextSeq500/550 or NovaSeq6000 (Illumina, San Diego, CA, USA). For details, see Supp. Methods.

Variants were classified according to ACMG criteria[13] and refer to NCBI transcript GRCh37 NM_000053.4.

2.3 | Vector constructs

pcDNA3 ATP7B expression vectors containing the coding region of the *ATP7B* gene (NM_000053.4) were generated by PCR. pcDNA3.1 RUNX1c (kindly provided by Tim Ripperger, MHH, Hannover, Germany) was used as transfection control for western blot analyses.

The different *ATP7B* variants were introduced using the QuickChange lightning site-directed mutagenesis kit (Agilent Technologies, Santa Clara, CA, USA). For details, see Supp. Methods.

For construction of a copper-sensitive firefly luciferase reporter vector, a sequence containing four tandem repeats of metal responsive element d of the mouse metallothionein I[19] promotor and a TATA box was synthesized by genscript (Piscataway, NJ, USA) and introduced into pGL3 basic vector (Promega, Mannheim, Germany). For details, see Supp. Methods.

2.4 | Cell culture

See Supp. Methods.

2.5 | Transfection

To overexpress ATP7B or its mutants for qRT-PCR measurements and western blot, HEK293T or Huh7 cells were seeded and transfected after 24 h with the respective pcDNA3_ATP7B vector (and pcDNA3.1_RUNX1c wild-type transfection control vector in case of protein lysates) using Lipofectamine 2000 (Thermo Fisher,

Braunschweig, Germany). The empty vector pcDNA3 served as negative control for ATP7B. For details, see Supp. Methods.

2.6 | mRNA analysis

RNA was transcribed into cDNA using the High-Capacity cDNA Reverse Transcription Kit (Thermo Fisher). Relative mRNA expression was measured using Taqman Gene Expression Assays (Thermo Fisher) using TATA box-binding protein (*TBP*) as a reference gene. Quantification was performed using the $2^{(-\Delta\Delta Ct)}$ method.

2.7 | Western blot

Harvested cells were lysed in RIPA buffer. After electrophoresis, proteins were transferred onto an Amersham Protran nitrocellulose membrane (Sigma/Merck, Darmstadt, Germany). The membrane was blocked for 1 h in non-fat milk and incubated with primary antibody (anti-Myc, abcam, Cambridge, UK, #ab9106; anti-RUNX1, Cell Signaling, Leiden, The Netherlands, #4334) over night at 4°C and secondary antibody (Goat anti rabbit IgG-HRP, abcam #ab6721, for ATP7B and goat anti-rabbit IgG-HRP, santa cruz, Dallas, Texas, USA, #sc-2054, for RUNX1) at room temperature for 1 or 2 h, respectively.

2.8 | Copper export capacity assay

HEK293T or Huh7 cells were seeded and transfected with pGL3 reporter construct, pRL-TK (Promega) and the respective pcDNA3_ATP7B vector after 24 h using Lipofectamine 2000. Cotransfected pRL-TK coding for Renilla luciferase served for normalization. 24 h after transfection, HEK293T and Huh7 cells were treated with 50 and 150 μM $CuCl_2$ (Sigma/Merck, #C3279), respectively. Luciferase activity was measured after additional 24 h with the Dual-Glo Luciferase Assay System (Promega) and normalized to Renilla luciferase activity. pcDNA3_GFP was used as an overexpression control, for which no effect on copper transport is expected. Copper export capacity of pcDNA3_GFP was set to 0 and that of pcDNA3_ATP7B_wild-type was set to 1. For details, see Supp. Methods.

2.9 | Immunofluorescence staining

HEK293T cells were seeded on poly-L-lysin coated cover slips 24 h before transfection with the respective pcDNA3_ATP7B vector using Lipofectamine 2000. The empty vector pcDNA3 served as negative control. After 24 h medium was changed to medium containing 50 μM of the copper chelator Bathocuproine disulfonic acid (Sigma/Merck, #146625). After additional 24 h, cells were washed in warm PBS and fixed for 10 min at room temperature using 4% paraformaldehyde, After washing with TBS and with PBS, cells were permeabilized for 25 min with 0.2% Triton-X 100 and blocked with 6% BSA and 0.2% Triton-X 100 for 1 h. Cells were incubated with rabbit anti-Myc antibody (abcam, #ab9106) together with either mouse anti-Golgin-97 (Invitrogen/Life Technologies, Carlsbad, USA, #A-21270) or mouse anti-Calnexin (Invitrogen, #MA3-027) antibody for 1 h in PBS with 1% BSA at room temperature. After washing, cells were incubated with secondary antibody goat anti-rabbit Alexa Fluor 488 (abcam, #ab150077) together with goat anti-mouse Alexa Fluor 594 (Invitrogen, #A-11032) for 1 h at room temperature. Cover slips were counterstained with DAPI (Sigma/Merck, #D8417). Staining was analyzed using Axio Imager M1 microscope (Zeiss, Oberkochen, Germany). For details, see Supp. Methods. Assigning the localization of the ATP7B-Myc signal to a certain compartment was based on evaluating at least 20 cells. Representative cells are shown in the corresponding figure.

2.10 | ATP7B protein structure modeling and folding free energy computations

The ATP7B amino acid sequence (Uniprot access number: P35670-1) was submitted to ColabFold,[20] a platform enabling AlphaFold v2.0,[21] to predict the ATP7B 3D structure. The obtained best model was taken for further analysis, namely structural impact estimation based on variant localization and changes in the folding free energy compared to the wild type protein using FoldX[22] and flex ddG[23] (which uses the Backrub method within the Rosetta framework to estimate free energy differences[24–26]). Images of wild type and variant proteins were generated using PyMol (Schrödinger, LLC, New York). The protein structure without the MBDs was first relaxed to remove potentially unfavorable contacts within the structure before calculating free energy differences using FoldX and flex ddG. For both methods, variants with an estimated folding free energy change of $\Delta\Delta G > 3$ kcal*mol^{-1} were considered highly destabilizing, variants with an estimate of $1 < \Delta\Delta G \leq 3$ kcal*mol^{-1} were considered destabilizing, and variants with an estimate of $-1 < \Delta\Delta G \leq 1$ kcal*mol^{-1} were considered neutral.[27] For details, see Supp. Methods.

3 | RESULTS

3.1 | Subjects and *ATP7B* variants

We studied *ATP7B* missense variants detected by next-generation whole exome or panel sequencing in six patients with clinically diagnosed WD (according to Leipzig score[28]: score ≥8) (Table 1). At the time point of manifestation, the patients were 5–16 years old. First symptoms ranged from elevated liver enzymes, neurologic seizures, or liver cirrhosis to acute liver failure. Two patients developed Kayser-Fleischer rings (Table 1, patient 1 + 5), and all except one (Table 1, patient 4), showed neuropsychiatric symptoms in the disease course ranging from tremor (Table 1, patient 1 + 2), speech developmental delay (Table 1, patient 6), or dystonia (Table 1, patient 3) to cerebral seizures with behavioral changes (Table 1, patient 5). In all cases (where it was investigated) increased liver copper

TABLE 1 Clinical characteristics of the patients and molecular characteristic of *ATP7B* variants.

Patient	1	2	3	4	5	6
Family	a	b	c	d	d	e
Sex	f	f	m	f	m	f
Age at manifestation	8 years	16 years	7 years	13 years	11 years	5 years
First symptoms	Liver cirrhosis	Elevated liver enzymes	Elevated liver enzymes	Acute liver failure	Neurologic/ seizure	Elevated liver enzyms
Kayser Fleischer rings	Yes (2)	No (0)	No (0)	No (0)	Yes (2)	No (0)
Neuropsychiatric symptoms	Tremor, reduced school performance (1)	Tremor (1)	Dystonia (right arm and hand), ADHD (1)	No (0) (hepatic encephalopathy due to acute liver failure)	Cerebral seizures, focal lesions in cMRI, behavioral changes (2)	Develop-mental delay, especially speech (1)
Serum ceruloplasmin	55 mg/L (2)	40 mg/L (2)	100 mg/L (1)	94 mg/L (2)	29 mg/L (2)	< 30 mg/L (2)
(norm 160–450 mg/L)						
Coombs negative hemolytic anemia	No (0)	No (0)	No (0)	Yes (2)	No (0)	No (0)
Liver copper content	Not done	746 µg/g (2)	1092 µg/g (2)	918 µg/g (2)	903 µg/g (2)	1350 µg/g (2)
(Norm <50 µg/g)						
Rhodamin-pos. Granula	Not done	Yes	Yes	Yes	Yes	Yes
24 h urinary copper	>8 ULN (2)	>10 ULN (2)	Normal (0)	>10 ULN (2)	>8 ULN (2)	>10 ULN (2)
24 h urinary copper +penicillamine	>2 ULN	>2 ULN	Normal	Not done	>10 ULN	>10 ULN
Therapy	LTx	D Pen	D Pen	LTx	Trientine	D Pen
ATP7B variants	c.2537T>C p.(Leu846Pro) het VUS; c.2305A>G p.(Met769Val) het P (1)	c.2596A>G p.(Lys866Glu) het VUS; c.3031G>T p.(Gly1011*) het P (1)	c.3053C>T p.(Ala1018Val) het LP; c.4042_4043delGT, p.(Ile1348Cysfs*29) het LP (4)	c.3188C>T p.(Ala1063Val) hom LP (4)	c.3188C>T p.(Ala1063Val) hom LP (4)	c.3912G>T p.(Leu1304Phe) hom LP (4)
Leipzig score[12]	8	8	8	12	14	11

Note: Variants refer to NCBI transcript GRCh37 NM_000053.4, numbers in brackets represent points for the Leipzig score.[12]

Abbreviations: ADHD, attention deficit hyperactivity disorder; cMRI, cranial magnetic resonance imaging; D Pen, D-Penicillamine; f, female; het, heterozygous; hom, homozygous; (L)P, (likely) pathogenic; LTX, liver transplantation; m, male; ULN, upper limit of the normal; VUS, variant of unknown significance.

content (Table 1, patients 2–6) and decreased serum ceruloplasmin levels (Table 1, patients 1–6) were determined. All except one (Table 1, patient 3) showed increased urine copper. Patients 4 and 5 were siblings but had different phenotypes. Patient 4 initially presented with acute liver failure, whereas her brother showed severe neuropsychiatric symptoms. Two studied variants were novel and classified as VUS according to ACMG criteria prior to our analyses (c.2537T>C p.(Leu846Pro), c.2596A>G p.(Lys866Glu)). Variants c.3188C>T p.(Ala1063Val), c.3053C>T p.(Ala1018Val) and c.3912G>T p.(Leu1304Phe) were already classified as likely pathogenic. However, their pathomechanism was still unclear.

3.2 | Protein expression and/or copper export capacity was significantly decreased for some mutants

To gain further insight into the pathomechanism, we transiently overexpressed the different *ATP7B* variants of interest in the two cell lines HEK293T and Huh7. As pathogenic missense control we used the well-known variant c.3207C>A p.(His1069Gln) of ATP7B protein, which has already been described to result in partly retention in the ER, a decreased protein level due to endoplasmic reticulum (ER)–associated degradation (ERAD) and slightly decreased copper transport activity.[29–32] As loss-of-function control, we used the known nonsense variant c.915T>A p.(Cys305*)[33,34] that is expected to result in a truncated protein (premature stop in exon 2) in our expression system. As benign control, we used the common variant c.3620A>G p.(His1207Arg) (total minor allele frequency in gnomAD: 2.86%, https://gnomad.broadinstitute.org/variant/13-52513266-T-C).

Western blots were performed to analyze whether the mutant proteins were expressed at normal levels or whether they might be subjected to degradation due to ERAD (Figure 1A). Prior to the western blot, qRT-PCR analyses confirmed that the transient transfection led to an overexpression on the mRNA level for all variants (Supp. Results Figure 2). The wild type and the benign control p.(His1207Arg) showed high protein expression on a comparable level, whereas p.(Leu846Pro), p.(Ala1063Val) and p.(Leu1304Phe) showed only weak or no bands in both cell lines. The variants p.(Lys866Glu) and p.(Ala1081Val) showed clearly detectable bands but were weaker than the wildtype. To examine whether the variants of interest have an effect on the copper transport, we performed copper export capacity assays (Figure 1B) using the firefly luciferase driven by a copper sensor as a reporter. The sensor was based on metal-responsive elements of the mouse metallothionein-1 promotor cloned upstream of the

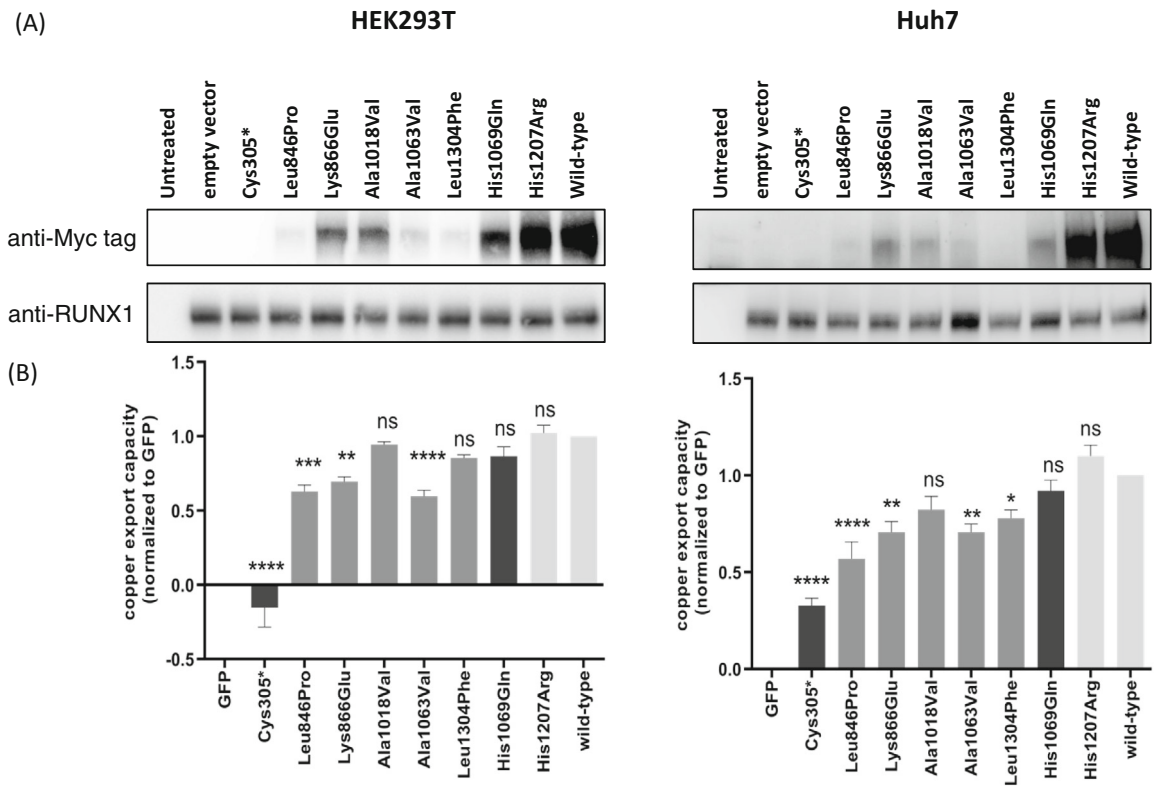

FIGURE 1 Protein expression and/or copper export capacity was significantly decreased for some mutants. (A) Western blot of HEK293T and Huh7 cells after transient co-transfection with the vector containing the indicated *ATP7B* variant and RUNX1 wild-type vector as transfection control. (B) Copper export capacity of HEK293T and Huh7 cells after co-transfection with pGL3_4MRE, pRL-TK and pcDNA3_empty vector, pcDNA3_GFP or pcDNA3_ATP7B wildtype/mutants. Data is based on least 3 biological replicates with 3 technical replicates each. Statistics: one-way ANOVA/Dunnet's Multiple Comparison Test, ns: $P > 0.05$; *$P \leq 0.05$; **$P \leq 0.01$; ***$P \leq 0.001$; ****$P < 0.0001$. Error bars show standard deviation. Dependence of luciferase activity on copper concentration is shown in Supp. Results Figure 1.

firefly luciferase open reading frame. Except for p.(Ala1063Val), all variants of interest led to significantly decreased copper export capacity values in at least one cell line. Values for the wild type and the benign control p.(His1207Arg) were similar (1 and 1.02 in HEK293T and 1 and 1.1 in Huh7, respectively), whereas the pathogenic truncating control variant p.(Cys305*) showed the strongest reduction in both cell lines (−0.15 in HEK293T and 0.32 in Huh7). Interestingly, the pathogenic missense control p.(His1069Gln) showed only a slight, statistically non-significant reduction (to 0.86 in HEK293T and to 0.92 in Huh7) which, however, has been similarly observed by others.[30]

3.3 | Immunofluorescence staining showed (partly) ER retention for most of the mutants

To investigate if the mutants were able to reach the TGN – the compartment where ATP7B is localized under physiological low copper conditions – or were trapped in the ER, we performed immunofluorescence staining (Figure 2). The wildtype and the benign control p.(His1207Arg) showed distinct co-staining with the TGN marker Golgin-97 (Figure 2, left panel). We observed similar co-staining for the mutant p.(Ala1018Val). The mutant p.(Lys866Glu) showed a predominant co-staining with the TGN marker (Figure 2, left panel), but in part also a co-staining with the ER marker Calnexin (Figure 2, right panel). The mutants p.(Leu846Pro) and p.(Leu1304Phe) as well as the pathogenic missense control, p.(His1069Gln), the latter known to be partly retained in the ER, showed mainly a co-staining with the ER marker (Figure 2, right panel), but in part also co-staining with the TGN marker (Figure 2, left panel). The mutant p.(Ala1063Val) showed a strong ER co-staining (Figure 2, right panel) without clear co-staining for the TGN marker (Figure 2, left panel).

3.4 | Predictions of the structural impact and folding free energy calculations indicated changed interaction patterns and impaired protein stability for most of the mutants

In order to evaluate the impact of variants from a structural perspective, we generated a structural ATP7B model with ColabFold,[20] a platform for AlphaFold-based protein structure predictions.[21] The location of variant sites is shown in Figure 3, together with a detailed structure-based analysis of the variant impact based on the local structural environment, functionally important motifs and literature knowledge. The changed interaction patterns due to the amino acid exchange are depicted in Supp. Results Figure 4.

Since variants often lead to changes in the stability of the folded protein, we further analyzed the folding free energy changes ($\Delta\Delta G$) between a variant and the wildtype using FoldX[22] and flex ddG.[23] Either method computes $\Delta\Delta G$ after substituting the wild type residue with the variant one, followed by a structural relaxation. Note that the variant impact on the unfolded state, the folding pathway, or the transport of the folded variant from the ER to the TGN and apical membrane cannot be deduced from this analysis. $\Delta\Delta G$ computed by FoldX indicated that the substitutions are "destabilizing" or "highly destabilizing" for all variants except p.(Ala1063Val). Furthermore, the variant p.(Leu846Pro) showed a significantly larger (p-value $= 2.6{*}10^{-8}$; Mann–Whitney-U test) destabilization than the average over all substitutions of this residue using the FoldX method (1.76 ± 0.02 kcal*mol^{-1}). Conversely, predictions by flex ddG classified all variants as neutral, potentially due to the different relaxation protocols used or due to the different energy scoring functions (see Supp. Methods). Overall, variants were considered destabilizing when at least one of the methods yielded a destabilizing classification[35] (Table 2). As such, all variants except for p.(Ala1063Val) were predicted to be destabilized, with p.(Ala1018Val) showing the smallest destabilizing effect.

4 | DISCUSSION

Our functional analyses could show that a pathogenic effect is highly likely for the two investigated VUS p.(Leu846Pro) and p.(Lys866Pro) so that the genetic cause of the clinical WD diagnosis is now identified. The other three variants could already be classified as likely pathogenic before our analyses as they were not novel. Especially p.(Ala1018Val) and p.(Ala1063Val) have been detected in multiple WD patients (Supp. Results Table 2). Two of the three variants can now be reclassified from likely pathogenic to pathogenic. Although this reclassification has no direct clinical consequences, our functional analyses allow deeper insights into the variant's pathomechanism, which could become relevant in terms of future targeted therapy. Table 3 gives an overview of the functional consequences of all variants of interest. Supp. Results Table 2 shows the ACMG classification before and after our analyses. Variant details are discussed in the following:

The novel variant p.(Leu846Pro), localized in the actuator domain, led to a significantly decreased protein level, copper export capacity (Figure 1), and co-staining with the ER marker. A small protein proportion was detected to reach the TGN (Figure 2). Therefore, the pathomechanism of p.(Leu846Pro) is likely based on a decreased protein level and ER mislocalization but possibly also in part by impaired protein function due to disfavored β-sheet secondary structure (Figure 3), likely resulting in a highly destabilized protein predicted by FoldX (Table 2).

The novel variant p.(Lys866Glu), also localized in the actuator domain, led to a slightly decreased protein level. However, the copper export capacity was massively decreased (Figure 1). The overexpressed protein mainly colocalized with the TGN marker but could, in part, also be detected in the ER (Figure 2). These data in conjunction with the protein structural data allow the assumption that the variant decreases the dephosphorylation activity by impairing the TGE-motif (Figure 3), potentially through local destabilizing effects (Table 2). Mislocalization and protein level may play a subordinate role.

The variant p.(Ala1018Val), localized in the P-domain, was already classified as likely pathogenic prior to this study and was detected in multiple WD patients (Supp. Results Table 2). We observed that the mutant protein correctly localized in the TGN (Figure 2). We detected an only slightly reduced ATP7B protein level and slightly reduced copper export capacity, which was not statistically significant but in the

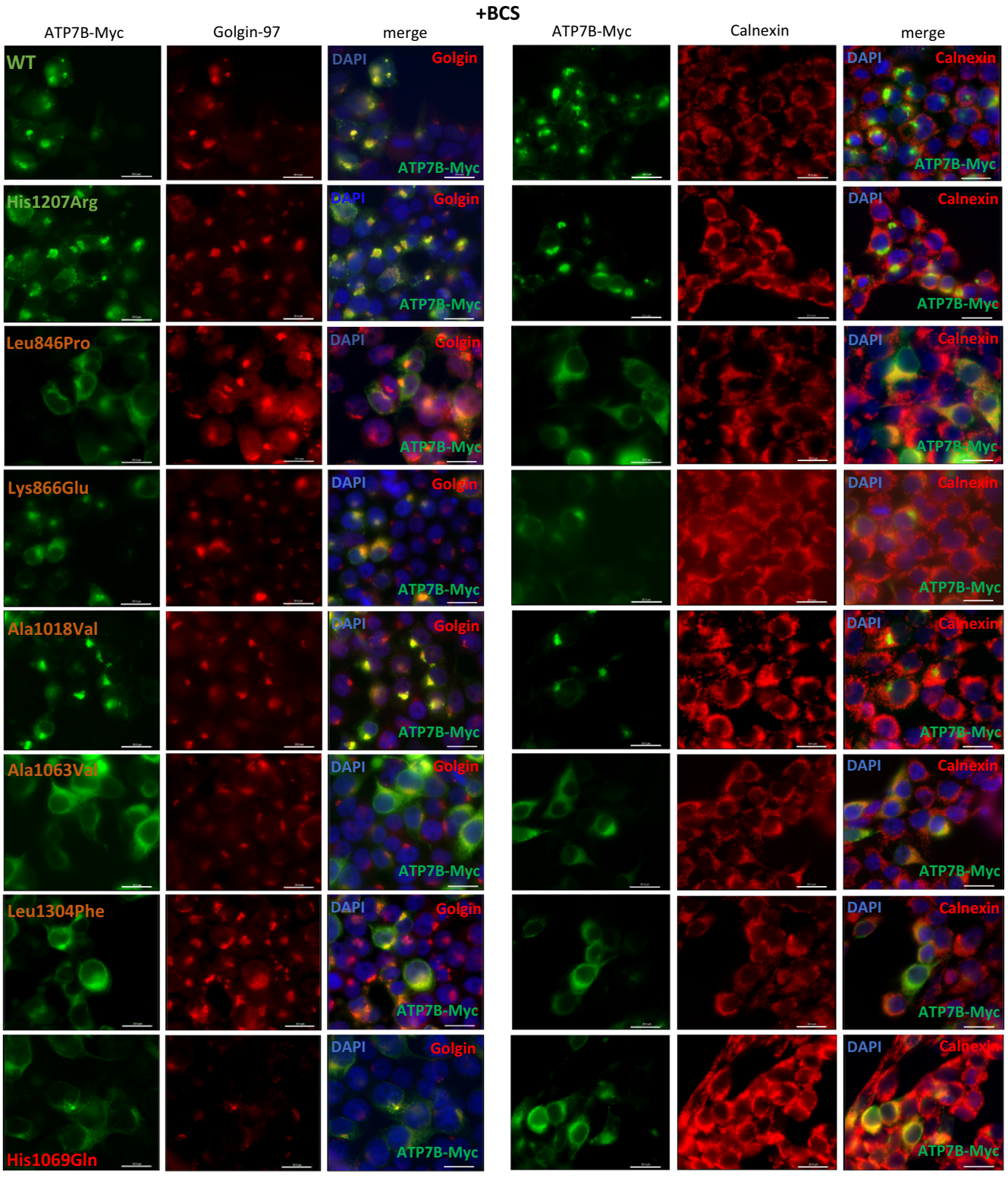

FIGURE 2 Immunofluorescence staining showed ER retention for some mutants. Immunofluorescence staining of HEK293T cells after transient transfection with the vector containing the indicated *ATP7B* variant and Bathocuproine disulfonic acid (BCS) treatment. The left three columns show MYC-tagged ATP7B (green), Golgin-97 as trans-Golgi network (TGN) marker (red) and merged images to determine co-localization. The right three columns show MYC-tagged ATP7B (green), Calnexin as endoplasmic reticulum (ER) marker (red) and merged images to determine co-localization. Original magnification ×630, scale bar in the bottom right corner ≙20 μm. Staining for pcDNA3 empty vector control and pathogenic truncating control variant p.(Cys305*) is shown in Supp. Results Figure 3. [Colour figure can be viewed at wileyonlinelibrary.com]

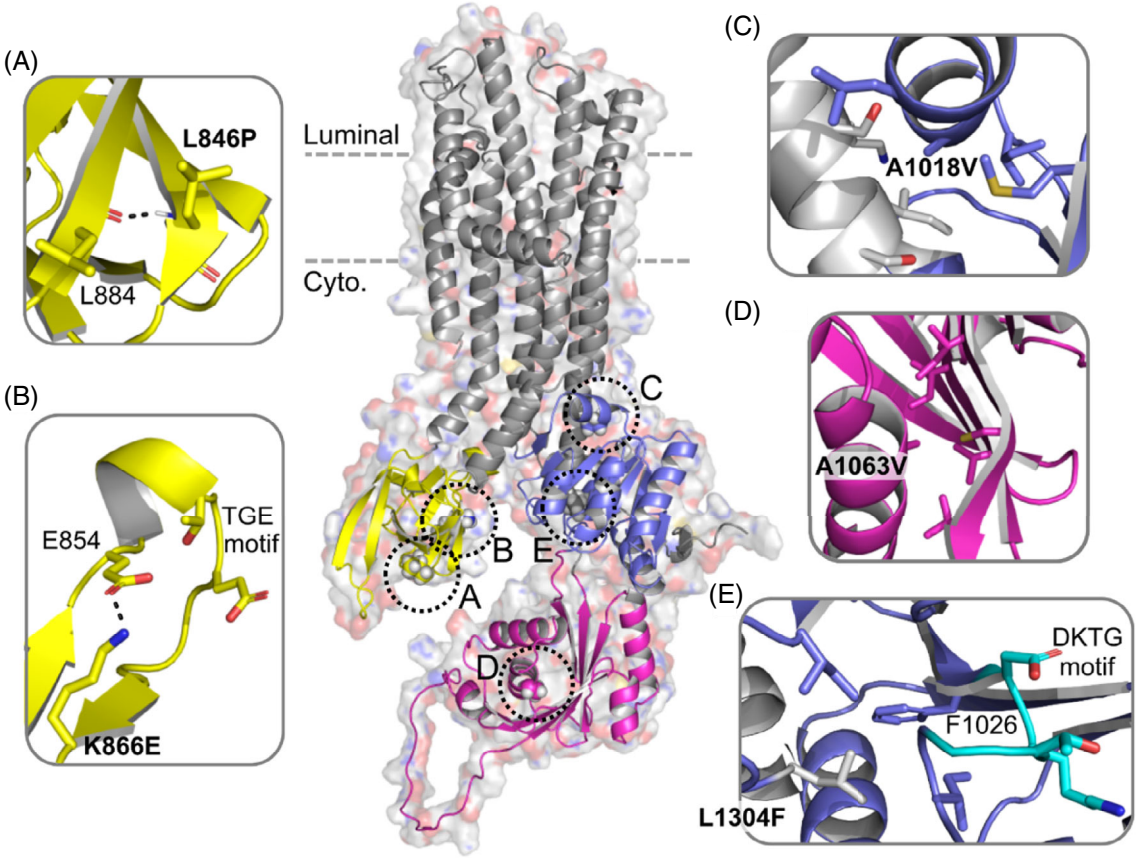

Variant	Localization	Potential effect
L846P	A-domain	L846, located on a β-strand, forms a backbone hydrogen bond with L884 on a neighboring antiparallel β-strand. Variant P846 cannot form the backbone hydrogen bond and disfavors the β-sheet secondary structure.
K866E	A-domain	K866 can form a salt bridge with residue E854; variant E866 would be repelled by E854. The TGE motiflies between the two interacting residues, which is important for the dephosphorylation of the transiently phosphorylated residue D1027[41-43]. The variant likely decreases the dephosphorylation activity.
A1018V	P-domain	A1018 is located on a short α-helix, facing toward the interface between the P-domain and TMH5. The larger variant V1018 might impact the movement of the P-domain during the dynamic cycle of copper transport[43].
A1063V	N-domain	A1063 is located on an α-helix, facing toward the mainly hydrophobic core of the N-domain. The (invariant in P_1-type ATPases) SEHPL motifis at the C-terminal end of this α-helix, which is important for ATP binding[37]. This motif also contains a well-studied variant leading to WD, H1069Q, which revealed that H1069 is important for nucleotide coordination; substitutions to amino acids Q, A, or C did not lead to incorrect folding of ATP7B[37]. The variant V1063 potentially influences SEHPL motif positioning due to its larger size compared to the wild-type. Close-by residues have been additionally identified as variant sites in WD, namely G1061E and E1064K[44,45], indicating the importance of the region. However, as the effect differs (E1064K leads to inactive protein with no phosphorylation activity[45], while G1061E is trapped in the ER[44]) between variants, and the property changes are larger for the variants G1061E and E1064K than the variant A1063V, no prediction can be inferred from this knowledge.
L1304F	TMH5	L1304 is located at the cytosolic end of TMH5, facing toward the P-domain, with the loop containing the conserved DKTG motifin proximity. The phosphorylation DKTG motif contains the catalytic D1027, which transiently undergoes phosphorylation during the catalysis cycle[1,43]. As such, the positioning of this motif will be crucial for protein activity. The variant F1304 can form π-π interactions with the residue F1026, potentially displacing the catalytic D1027 from a perfect placement for transient phosphorylation. The importance of residue F1026 is further corroborated through a known WD-causing variant, F1026Y[46].

FIGURE 3 Protein structure model of ATP7B and localization of variants. The protein model of ATP7B was generated using ColabFold.[20] Metal binding domains (MBDs) were excluded for better visualization of the variant sites. A-domain, P-domain, and N-domain are colored yellow, blue, and magenta, respectively. The location of the membrane is indicated by gray dotted lines. (A) Variant site of p.(Leu846Pro), located within the A-domain on a β-strand. The wildtype amino acid Leucine can form a hydrogen bond via the hydrogen on the backbone nitrogen of Leu846 with the oxygen of the backbone of Leu884, as indicated by the dotted line (distance: 1.8 Å). (B) Variant site of p.(Lys866Glu), which is located within the A-domain close to the TGE motif necessary for dephosphorylation of the catalytic residue. The wildtype amino acid Lysine forms a salt bridge with residue Glu854, as indicated by the dotted line (2.7 Å), measured with PyMol. (C) Variant site of p.(Ala1018Val), located within the P-domain in a short α-helix. (D) Variant site of p.(Ala1063Val), located within the N-domain in an α-helix, with the sidechain facing the core of the domain. (E) Variant site of p.(Leu1304Phe), located at the beginning of transmembrane helix 5 (TMH5) and facing towards the P-domain, including the DKTG motif, which contains the intermediate phosphorylation site. [Colour figure can be viewed at wileyonlinelibrary.com]

TABLE 2 Prediction of folding free energy changes of variants. Variant impact on the folding free energy compared to wildtype was predicted using FoldX and flex ddG. Values represent mean ± standard deviation.

Variant	FoldX ΔΔG (kcal mol^{-1})	Classification FoldX	flex ddG ΔΔG (kcal mol^{-1})	Classification flex ddG	Overall classification
L846P	7.69 ± 0.10	Highly destabilizing	0.00 ± 0.05	Neutral	Destabilizing
K866E	2.99 ± 0.08	Destabilizing	0.07 ± 0.06	Neutral	Destabilizing
A1018V	1.13 ± 0.13	Destabilizing	−0.01 ± 0.05	Neutral	Destabilizing
A1063V	0.71 ± 0.17	Neutral	0.00 ± 0.06	Neutral	Neutral
L1304F	2.60 ± 0.48	Destabilizing	−0.04 ± 0.07	Neutral	Destabilizing
H1069Q	1.01 ± 0.05	Destabilizing	0.01 ± 0.04	Neutral	Destabilizing
H1207R	−0.31 ± 0.11	Neutral	0.00 ± 0.02	Neutral	Neutral

Note: Variants were considered destabilizing when at least one of the methods yielded a destabilizing classification. Uniprot access number: P35670-1.

TABLE 3 Overview of the functional characteristics and protein model-based predictions of the variants.

ATP7B variant	Protein level in western blot	Copper export capacity	IF co staining	Predicted effect based on folding free energy changes
c.3620A>G p.(His1207Arg) Benign control	+	+	**TGN**	Neutral
c.2537T>C p.(Leu846Pro)	–	–	**ER**/TGN	Destabilizing
c.2596A>G p.(Lys866Glu)	–	–	**TGN**/ER	Destabilizing
c.3053C>T p.(Ala1018Val)	–	–†	TGN	Destabilizing
c.3188C>T p.(Ala1063Val)	–	–	ER	Neutral
c.3912G>T p.(Leu1304Phe)	–	–	**ER**/TGN	Destabilizing
c.3207C>A p.(His1069Gln)	–	–†	TGN/ER	Destabilizing
Pathogenic missense control				
c.915T>A p.(Cys305*) Pathogenic nonsense control	No band detectable (AB directed against C-terminal MYC-tag)	–	No specific signal (AB directed against C-terminal MYC-tag)	n.a.

Note: + Comparable to wild-type; – Decreased (Number of "–" indicates degree of reduction); † Statistically not significant. Bold type indicates predominant cellular localization. Variants refer to NCBI transcript GRCh37 NM_000053.4.
Abbreviations: AB, antibody; ER, endoplasmic reticulum; IF, immunofluorescence; n.a. not applicable; TGN, trans-Golgi network.

same range as the pathogenic control p.(His1069Gln) (Figure 1). Van den Berghe et al. have also observed an only modestly reduced copper export capacity for p.(His1069Gln) in this type of assay (~0.75)[30] and Das et al. have described similar results for p.(His1069Gln) copper transport using tyrosinase assay.[32] For p.(His1069Gln), the main pathomechanism appears to be ERAD, while it was partly able to reach the TGN.[29] Possibly, the ATP7B protein fraction able to reach the TGN is enough to maintain copper transport to a large extent in our assay. This could indicate that even small reductions in our assay show a pathogenic, but potentially modest effect.[37] Based on the protein structure and the positioning at the interface of the P-domain to the TMHs, p.(Ala1018Val) might impair movement of the P-domain during the dynamic cycle (Figure 3). FoldX analysis predicted a destabilizing effect of p.(Ala1018Val), but with a folding free energy change (1.13 ± 0.13 kcal*mol^{-1}) only slightly above the threshold for neutral effect ($-1 < \Delta\Delta G \leq 1$ kcal*mol^{-1}), which is, similar to p.(His1069Gln) (1.01 ± 0.05 kcal*mol^{-1}) (Table 2), in line with our in vitro data. Several publications have described WD patients carrying heterozygous p.(Ala1018Val) together with another *ATP7B* variant (Supp. Results Table 2) as our patient 3. However, we could identify only one report of a patient with p.(Ala1018Val) in the homozygous state (together with another homozygous *ATP7B* VUS).[36] Interestingly, this patient presented with relatively late age of onset (43 years), which underlines the assumption that this variant likely results in only modest effects. However, so far there are no clear data showing genotype–phenotype correlations in WD. First indications for such a correlation for p.(His1069Gln) could be disproved in a study with larger numbers of cases.[9] As the copper export capacity data were statistically not significant and the cellular localization appeared to be normal, we refrained from applying ACMG criterion PS3 for the variant. However, we cannot exclude that the translocation of the protein to the plasma membrane under high copper concentration was impaired. Furthermore, the variant could also influence splicing, which cannot be addressed with the intron-less expression vector used in our assays.

The variant p.(Ala1063Val), already detected in several WD patients (Supp. Results Table 2) and classified as likely pathogenic prior to this study, was localized in the N-domain. It led to a

significantly decreased protein level and copper export capacity in our assays (Figure 1). Immunofluorescence staining revealed a complete co-staining with the ER marker (Figure 2). The variant is localized in an α-helix close to the SEPHL motif (Figure 3). This motif is important for ATP binding[37] and harbors the pathogenic missense control variant p.(His1069Gln). The variant p.(Ala1063Val) potentially influences the SEPHL motif positioning (Figure 3). However, FoldX analysis of the folding free energy changes predicted a neutral effect (Table 2). This did not contradict the in vitro data, because the prediction was based on the final well-folded structure, and cannot predict the variant impact on the unfolded structure. The observed ER retention for p.(Ala1063Val) hints towards a complete misfolding "before" the predicted effects on the folded structure can take place. Therefore, we concluded that the pathomechanism of p.(Ala1063Val) probably relies mainly on ER retention and subsequent ERAD.

Variant p.(Leu1304Phe), located at the cytosolic end of TMH 5, was also classified as likely pathogenic prior to this study. It has only been described once in a homozygous state in a 13 year-old male with chronic liver disease[38] so far. We detected a reduced protein level and copper export capacity in our assays (Figure 1). The mutant showed co-staining with the ER marker. A small proportion of the protein was detected to reach the TGN (Figure 2). Therefore, the pathomechanism of p.(Leu1304Phe) is likely based on cellular mislocalization and decreased protein level, but possibly in part also on a displaced catalytic D1027 residue of the phosphorylation DKTG motif impairing transient phosphorylation (Figure 3). This is in accordance with a local destabilization of the protein as predicted by FoldX (Table 2).

Functional analyses are time-consuming. If the primary aim is to classify a variant as benign or pathogenic and mechanistic details are secondary, a curated classification approach, based on the Sherloc variant classification criteria, that systematically uses phenotypic evidence[39] may be considered. This is especially appropriate in WD, where the phenotype is often highly specific for the disease. However, with this approach, the larger the number of patients, the more weight can be given to the occurrence of a disease phenotype in combination with a rare variant as a sign of pathogenicity. For the two VUS analyzed in our study, this approach would not have led to reclassification as (likely) pathogenic without functional data, as they have not been described in other patients so far. Furthermore, functional analyses have the advantage of providing deeper insights into a variant's pathomechanism, which could help to develop future personalized therapies. Four of the five variants of interest were likely to destabilize the protein so that the catalytic cycle is impaired. However, three of these four appear to be – at least partly – trapped in the ER, likely leading to ERAD before transfer to TGN is possible. For these variants, therapeutic approaches targeting ERAD may improve, albeit not completely rescue the phenotype as they probably still lead to destabilized proteins. One variant p.(Ala1063Val) likely does not lead to protein destabilization but appears to be fully trapped and degraded in the ER. Here, interventions addressing ERAD, as pharmacological folding chaperones[30] or inhibitors of proteostasis-involved proteins, such as HSP70,[40] may be most promising. They could be a possible supplement or alternative to current therapies in case of side effects or insufficient efficacy in neuropsychiatric patients.

AUTHOR CONTRIBUTIONS

Study design: Amelie Stalke, Ulrich Baumann, Brigitte Schlegelberger, Thomas Illig, Eva-Doreen Pfister, Britta Skawran; data acquisition: Amelie Stalke, Annika Behrendt, Finja Hennig, Holger Gohlke, Nicole Buhl, Thea Reinkens, Eva-Doreen Pfister; data analysis and interpretation: Amelie Stalke, Annika Behrendt, Finja Hennig, Holger Gohlke; manuscript preparation: Amelie Stalke; critically reviewed by Annika Behrendt, Finja Hennig, Holger Gohlke, Nicole Buhl, Thea Reinkens, Brigitte Schlegelberger, Thomas Illig, Eva-Doreen Pfister, Britta Skawran.

ACKNOWLEDGMENTS

We thank Sonja Bockisch for medical care/providing samples for genetic analysis of patient 3 and Claudia Davenport for her help in manuscript editing. We are grateful for computational support and infrastructure provided by the "Zentrum für Informations- und Medientechnologie" (ZIM) at the Heinrich Heine University Düsseldorf and the computing time provided by the John von Neumann Institute for Computing (NIC) to HG on the supercomputer JUWELS at Jülich Supercomputing Centre (JSC) (user ID: VSK33, FIC1). Open Access funding enabled and organized by Projekt DEAL.

FUNDING INFORMATION

Supported by the German Research Foundation (DFG) (project #433387263 to Amelie Stalke) and, in part, by the German Federal Ministry for Education and Research (BMBF) through HiChol (01GM1904A to Holger Gohlke).

CONFLICT OF INTEREST STATEMENT

Advisory boards (Ulrich Baumann, Eva Doreen Pfister), grant support (Ulrich Baumann): Alexion, with no role in study design, collection, analysis, interpretation of data, report writing and in decision to publish the report; Amelie Stalke, Annika Behrendt, Finja Hennig, Holger Gohlke, Nicole Buhl, Thea Reinkens, Brigitte Schlegelberger, Thomas Illig, Britta Skawran declare no conflict of interest.

DATA AVAILABILITY STATEMENT

Patient and variant information can be found at https://databases.lovd.nl/shared/individuals/ATP7B (Individuals #00427853 to #00427858).

ORCID

Amelie Stalke https://orcid.org/0000-0002-8438-8692

REFERENCES

1. Møller JV, Juul B, le Maire M. Structural organization, ion transport, and energy transduction of P-type ATPases. *Biochim Biophys Acta*. 1996;1286(1):1-51.
2. Wu CC, Rice WJ, Stokes DL. Structure of a copper pump suggests a regulatory role for its metal-binding domain. *Structure*. 2008;16(6):976-985.
3. Tsivkovskii R, Eisses JF, Kaplan JH, Lutsenko S. Functional properties of the copper-transporting ATPase ATP7B (the Wilson's disease protein) expressed in insect cells. *J Biol Chem*. 2002;277(2):976-983.

4. Sazinsky MH, Mandal AK, Argüello JM, Rosenzweig AC. Structure of the ATP binding domain from the Archaeoglobus fulgidus Cu +-ATPase. *J Biol Chem*. 2006;281(16):11161-11166.
5. Banci L, Bertini I, Cantini F, et al. Solution structures of the actuator domain of ATP7A and ATP7B, the Menkes and Wilson disease proteins. *Biochemistry*. 2009;48(33):7849-7855.
6. Ramos D, Mar D, Ishida M, et al. Mechanism of copper uptake from blood plasma ceruloplasmin by mammalian cells. *PLoS One*. 2016; 11(3):e0149516.
7. Polishchuk R, Lutsenko S. Golgi in copper homeostasis: a view from the membrane trafficking field. *Histochem Cell Biol*. 2013;140(3): 285-295.
8. Polishchuk EV, Concilli M, Iacobacci S, et al. Wilson disease protein ATP7B utilizes lysosomal exocytosis to maintain copper homeostasis. *Dev Cell*. 2014;29(6):686-700.
9. Ferenci P, Stremmel W, Członkowska A, et al. Age and sex but not ATP7B genotype effectively influence the clinical phenotype of Wilson disease. *Hepatology*. 2019;69(4):1464-1476.
10. Kim JW, Kim JH, Seo JK, et al. Genetically confirmed Wilson disease in a 9-month old boy with elevations of aminotransferases. *World J Hepatol*. 2013;5(3):156-159.
11. Ala A, Borjigin J, Rochwarger A, Schilsky M. Wilson disease in septuagenarian siblings: raising the bar for diagnosis. *Hepatology*. 2005; 41(3):668-670.
12. Ferenci P, Caca K, Loudianos G, et al. Diagnosis and phenotypic classification of Wilson disease. *Liver Int*. 2003;23(3):139-142.
13. Richards S, Aziz N, Bale S, et al. Standards and guidelines for the interpretation of sequence variants: a joint consensus recommendation of the American College of Medical Genetics and Genomics and the Association for Molecular Pathology. *Genet Med*. 2015;17(5): 405-424.
14. Sánchez-Monteagudo A, Álvarez-Sauco M, Sastre I, et al. Genetics of Wilson disease and Wilson-like phenotype in a clinical series from eastern Spain. *Clin Genet*. 2020;97(5):758-763.
15. Nolan DK, Chaudhari B, Franklin SJ, et al. Hypomorphic alleles pose challenges in rare disease genomic variant interpretation. *Clin Genet*. 2021;100(6):775-776.
16. Wallace DF, Dooley JS. ATP7B variant penetrance explains differences between genetic and clinical prevalence estimates for Wilson disease. *Hum Genet*. 2020;139(8):1065-1075.
17. Mohr I, Weiss KH. Current anti-copper therapies in management of Wilson disease. *Annal Transl Med*. 2019;7(Suppl 2):S69.
18. Dev S, Kruse RL, Hamilton JP, Lutsenko S. Wilson disease: update on pathophysiology and treatment. *Front Cell Dev Biol*. 2022;10:871877.
19. Stuart GW, Searle PF, Chen HY, Brinster RL, Palmiter RD. A 12-base-pair DNA motif that is repeated several times in metallothionein gene promoters confers metal regulation to a heterologous gene. *Proc Natl Acad Sci U S A*. 1984;81(23):7318-7322.
20. Mirdita M, Schütze K, Moriwaki Y, Heo L, Ovchinnikov S, Steinegger M. ColabFold: making protein folding accessible to all. *Nat Methods*. 2022;19(6):679-682.
21. Jumper J, Evans R, Pritzel A, et al. Highly accurate protein structure prediction with AlphaFold. *Nature*. 2021;596(7873):583-589.
22. Schymkowitz J, Borg J, Stricher F, Nys R, Rousseau F, Serrano L. The FoldX web server: an online force field. *Nucleic Acids Res*. 2005; 33(Web Server issue):W382-W388.
23. Barlow KA, S ÓC, Thompson S, et al. Flex ddG: Rosetta Ensemble-based estimation of changes in protein-protein binding affinity upon mutation. *J Phys Chem B*. 2018;122(21):5389-5399.
24. Fleishman SJ, Leaver-Fay A, Corn JE, et al. RosettaScripts: a scripting language interface to the Rosetta macromolecular modeling suite. *PLoS One*. 2011;6(6):e20161.
25. Leaver-Fay A, O'Meara MJ, Tyka M, et al. Scientific benchmarks for guiding macromolecular energy function improvement. *Methods Enzymol*. 2013;523:109-143.
26. Smith CA, Kortemme T. Backrub-like backbone simulation recapitulates natural protein conformational variability and improves mutant side-chain prediction. *J Mol Biol*. 2008;380(4):742-756.
27. Tokuriki N, Stricher F, Schymkowitz J, Serrano L, Tawfik DS. The stability effects of protein mutations appear to be universally distributed. *J Mol Biol*. 2007;369(5):1318-1332.
28. Ferenci P. Diagnosis of Wilson disease. *Handb Clin Neurol*. 2017;142: 171-180.
29. Parisi S, Polishchuk EV, Allocca S, et al. Characterization of the most frequent ATP7B mutation causing Wilson disease in hepatocytes from patient induced pluripotent stem cells. *Sci Rep*. 2018;8(1):6247.
30. van den Berghe PV, Stapelbroek JM, Krieger E, et al. Reduced expression of ATP7B affected by Wilson disease-causing mutations is rescued by pharmacological folding chaperones 4-phenylbutyrate and curcumin. *Hepatology*. 2009;50(6):1783-1795.
31. Huster D, Hoppert M, Lutsenko S, et al. Defective cellular localization of mutant ATP7B in Wilson's disease patients and hepatoma cell lines. *Gastroenterology*. 2003;124(2):335-345.
32. Das S, Mohammed A, Mandal T, et al. Polarized trafficking and copper transport activity of ATP7B: a mutational approach to establish genotype-phenotype correlation in Wilson disease. *Hum Mutat*. 2022;43:1408-1429.
33. Loudianos G, Dessì V, Lovicu M, et al. Further delineation of the molecular pathology of Wilson disease in the Mediterranean population. *Hum Mutat*. 1998;12(2):89-94.
34. Stalke A, Pfister ED, Baumann U, et al. Homozygous frame shift variant in ATP7B exon 1 leads to bypass of nonsense-mediated mRNA decay and to a protein capable of copper export. *Eur J Hum Genet*. 2019;27(6):879-887.
35. Jayaraman K, Trachtmann N, Sprenger GA, Gohlke H. Protein engineering for feedback resistance in 3-deoxy-D-arabino-heptulosonate 7-phosphate synthase. *Appl Microbiol Biotechnol*. 2022;106(19–20): 6505-6517.
36. Annamalai AK, Prajna VN, Chowdhury G, et al. Wilson disease: never too late. *Am J Med*. 2022;135(9):e370-e371.
37. Tsivkovskii R, Efremov RG, Lutsenko S. The role of the invariant His-1069 in folding and function of the Wilson's disease protein, the human copper-transporting ATPase ATP7B. *J Biol Chem*. 2003; 278(15):13302-13308.
38. Møller LB, Horn N, Jeppesen TD, et al. Clinical presentation and mutations in Danish patients with Wilson disease. *Eur J Hum Genet*. 2011;19(9):935-941.
39. Johnson B, Ouyang K, Frank L, et al. Systematic use of phenotype evidence in clinical genetic testing reduces the frequency of variants of uncertain significance. *Am J Med Genet A*. 2022;188(9): 2642-2651.
40. Concilli M, Petruzzelli R, Parisi S, et al. Pharmacoproteomics pinpoints HSP70 interaction for correction of the most frequent Wilson disease-causing mutant of ATP7B. *Proc Natl Acad Sci U S A*. 2020; 117(51):32453-32463.
41. Jorgensen PL, Hakansson KO, Karlish SJ. Structure and mechanism of Na,K-ATPase: functional sites and their interactions. *Annu Rev Physiol*. 2003;65:817-849.
42. Clausen JD, Vilsen B, McIntosh DB, Einholm AP, Andersen JP. Glutamate-183 in the conserved TGES motif of domain a of sarcoplasmic reticulum Ca2+-ATPase assists in catalysis of E2/E2P partial reactions. *Proc Natl Acad Sci U S A*. 2004;101(9):2776-2781.
43. Bublitz M, Morth JP, Nissen P. P-type ATPases at a glance. *J Cell Sci*. 2011;124(Pt 15):2515-2519.
44. Roy S, McCann CJ, Ralle M, et al. Analysis of Wilson disease mutations revealed that interactions between different ATP7B mutants modify their properties. *Sci Rep*. 2020;10(1):13487.
45. Huster D, Kühne A, Bhattacharjee A, et al. Diverse functional properties of Wilson disease ATP7B variants. *Gastroenterology*. 2012;142(4): 947-956.e945.

46. Huong NTM, Lien NTK, Ngoc ND, et al. Three novel mutations in the ATP7B gene of unrelated Vietnamese patients with Wilson disease. *BMC Med Genet*. 2018;19(1):104.

SUPPORTING INFORMATION

Additional supporting information can be found online in the Supporting Information section at the end of this article.

How to cite this article: Stalke A, Behrendt A, Hennig F, et al. Functional characterization of novel or yet uncharacterized *ATP7B* missense variants detected in patients with clinical Wilson's disease. *Clinical Genetics*. 2023;104(2):174-185. doi:10.1111/cge.14352